Available online at www.sciencedirect.com
ScienceDirect
Polymer 49 (2008) 1015–1026
polymer
www.elsevier.com/locate/polymer

Fabrication and characterization of polyamide 6,6/organo-montmorillonite nanocomposites with and without a maleated polyolefin elastomer as a toughener

Fang-Chyou Chiu [a,*], Sheng-Wei Fu [a], Wei-Tsung Chuang [b], Hwo-Shuenn Sheu [b]

[a] *Department of Chemical and Materials Engineering, Chang Gung University, Tao-Yuan 333, Taiwan, ROC*
[b] *National Synchrotron Radiation Research Center, Hsinchu 300, Taiwan, ROC*

Received 7 September 2007; received in revised form 20 November 2007; accepted 25 November 2007
Available online 23 December 2007

Abstract

In this study, polyamide 6,6 (PA 6,6)-based nanocomposites were prepared using a twin-screw extruder. One commercial organo-montmorillonite (denoted as 30B) and one maleated polyolefin elastomer (denoted as POEMA) served as the reinforcing filler and toughener, respectively. The X-ray diffraction (XRD), scanning electron microscopy combined with energy dispersive spectroscopy (SEM/EDS), and transmission electron microscopy (TEM) results confirmed the nano-scaled dispersion of 30B in the composites. The presence of POEMA slightly depreciated the dispersibility of 30B. Differential scanning calorimetry (DSC) results indicated that the addition of 30B accelerated the crystallization of PA 6,6, whereas the simultaneous additions of 30B and POEMA led to a reverse effect. Complex melting behaviors, mainly associated with the "recrystallization/reorganization" of PA 6,6 crystals upon heating, were observed for neat PA 6,6 and the nanocomposites. The presence of exfoliated/intercalated 30B hampered the "recrystallization/reorganization" of PA 6,6 crystals. The thermal stability enhancement of PA 6,6 after the addition of 30B and/or POEMA was confirmed using thermogravimetric analysis (TGA). The rigidity, including storage modulus, Young's modulus and flexural modulus, of PA 6,6 increased after adding 30B. However, these properties declined after the further incorporation of POEMA. The PA 6,6/POEMA/30B nanocomposites basically displayed balanced properties between those of the neat PA 6,6 and PA 6,6/POEMA blend.

Keywords: PA 6,6; O-MMT; Nanocomposite

1. Introduction

The investigations on the fabrication and characterization of organic/inorganic nanocomposite systems have attracted much academic and industrial attention in the past decade. Among all the systems investigated, polymer/clay (silicate) composites have exhibited great promise for industrial applications due to their potential to display synergistically advanced properties with only minor amounts (e.g., 3–5 wt.%) of clay loading. The properties that have been demonstrated to be drastically enhanced include tensile/flexural strength, thermal stability, heat deflection temperature (HDT), flame retardancy, barrier property, and so on. The successful pioneering work on these nanocomposites was conducted on the polyamide 6 (PA 6)/montmorillonite (MMT) clay system by Toyota, Inc. [1,2]. Since then, intensive studies on the polymer/clay nanocomposite systems have been carried out [3–15].

According to the reported data, the above-mentioned MMT is recognized as an appropriate choice for manufacturing high performance polymer/clay nanocomposites. This naturally occurring clay displays a hydrophilic layered-structure comprised of 1-nm thin individual layers. These layers assemble themselves via specific interactions in a parallel manner to form a stacked (tactoid-like) arrangement in the micrometer scale. Due to the MMT's hydrophilic feature, using polar

* Corresponding author. Tel.: +886 3 2118800x5297; fax: +886 3 2118668.
E-mail address: maxson@mail.cgu.edu.tw (F.-C. Chiu).

0032-3861/$ - see front matter
doi:10.1016/j.polymer.2007.11.057

polymers as the matrix to develop MMT-included nanocomposites is feasible if the MMT surface is modified with certain organic surfactants (the modified MMT is thus denoted as O-MMT hereafter). The incorporation of organic surfactants will expand the MMT's interlayer spacing and also offer a positive enthalpic effect for mixing with organic polymers.

Polyamide 6,6 (PA 6,6) is one of the most widely used engineering polymers with a polar characteristic. It exhibits excellent thermal and mechanical properties, which makes it an important solution for many applications in the manufacture of construction materials and in the automotive parts and electronic industry, among others. Like most of the synthetic polymers, proper fillers and/or reinforcements are commonly incorporated into the PA 6,6 matrix to further improve its properties. Nevertheless, compared with PA 6-based and polyolefin-based nanocomposites, the researches conducted on PA 6,6-based nanocomposites are limited. Recently, some results were reported. Liu et al. [16] studied the phase transition and polymorphism of PA 6,6/O-MMT nanocomposites. They found that the introduction of O-MMT induced the appearance of γ-form PA 6,6 crystals in the nanocomposites. The Brill transition temperature of PA 6,6 was lowered with the incorporation of O-MMT. Nevertheless, in contrast, Yu et al. and Zhang et al. [17,18] reported that PA 6,6 mainly developed the stable triclinic α-form crystals in PA 6,6/O-MMT nanocomposites they prepared. Moreover, the Brill transition temperature of PA 6,6 was elevated with the incorporation of O-MMT. The effects of O-MMT content on reinforcement and fracture behavior of the nanocomposites were also evaluated. Kang et al. [19] indicated that the addition of intercalated O-MMT induced the β-form PA 6,6 crystals and also raised the crystallization temperatures of PA 6,6. Nair et al. [20] compared the fracture toughness of PA 6,6 composites with different types of O-MMTs and kaolin clay. They claimed that the special benefit of nanoscale reinforcement was derived from their high surface area of contact with the matrix. A better dispersion of the clay caused a higher toughness of the (nano)composites.

As anticipated, it was found from the above-mentioned literature that PA 6,6/organoclay nanocomposites could exhibit better stiffness and heat resistance in comparison with neat PA 6,6. Nevertheless, like PA 6/organoclay nanocomposite system, the impact strength (toughness) of PA 6,6 generally declined after the addition of organoclays. From a practical viewpoint, if PA 6,6/clay nanocomposites are to be used in numerous engineering applications, the ''low toughness'' deficiency should be overcome. It was reported that, to enhance the toughness of polyamides (e.g., PA 6 and PA 6,6), a low-modulus elastomeric component was usually incorporated into the polyamide matrix [21−27]. Among the elastomers used, maleated metallocene polyolefin elastomers (POEs) were evaluated to be the effective candidates [26,27]. Hitherto, little work was conducted on the toughening of PA 6,6/clay nanocomposites as far as we know. Thus, the main goal of this work is to examine the combined effects of adding an organoclay and a maleated metallocene POE on PA 6,6/clay composites fabrication and their mechanical properties. Additionally, as reported [16−19] the addition of organoclays might alter the crystal form development of PA 6,6. Accordingly, this work is to reveal the PA 6,6 crystal structure in the presence of an organoclay and/or a maleated POE as well. Moreover, the thermal properties, especially the complex melting behavior, of neat PA 6,6 and the fabricated composites were compared. One commercially available O-MMT and one maleic anhydride-grafted POE (POEMA) were used to melt-mix with PA 6,6 for the composites fabrication.

2. Experimental section

The PA 6,6 (trade name VYDYNE 21SP) used in this study is a commercial product of Solutia, Inc. Its relative viscosity is *ca*. 2.7. An O-MMT clay (Cloisite® 30B, denoted as 30B) obtained from Southern Clay Products, Inc. was used as the nano-filler for composite fabrication. The organic modifier for 30B is a methyl tallow bis-2-hydroxyethyl quaternary ammonium ion. The tallow composition is *ca*. 65% C18, 30% C16, and 5% C14. A POEMA with *ca*. 1 wt.% of MA, supplied by Nytex Composites Co. (Taiwan), was used as the toughener for the prepared PA 6,6/30B composites. The POEMA possesses a melt flow index of 9.1 g/10 min (at 230 °C and 2.16 kg load). The POE portion is a product (Engage® 8180) of Dupont Dow Elastomer Co.

All composites/blend were prepared through a melt-mixing procedure using an intermeshing twin-screw extruder (SHJ-20B, L/D = 40) in the co-rotating mode. The screw speed was maintained at 300 rpm. The barrel temperatures were kept at 220−265 °C from hopper to die. Before melt-mixing, the ingredients were dried for 24 h in an air-circulated oven to remove the absorbed water. The 30B content of the composites was kept at 3 and 5 wt.%, respectively. The POEMA was loaded at 15 wt.% if needed. Upon mixing, the ingredients were weighed at a certain ratio and then dry-mixed as one before feeding into the extruder. After mixing, the extruded samples were pelletized, followed by oven drying before further characterization. For comparison purposes, neat PA 6,6 was also melt-extruded under the same condition. The formulation and sample designations for the fabricated composites/blend are listed in Table 1.

X-ray diffraction (XRD) technique, scanning electron microscopy combined with energy dispersive spectroscopy (SEM/EDS), and transmission electron microscopy (TEM) were employed to assess the dispersibility of 30B in the composites. The crystal form of different thermally treated PA 6,6-based samples was determined by XRD as well. A Siemens

Table 1
Samples designation and formulations

Designation	Composition	Parts (wt.%)
Neat PA 6,6	PA 6,6	100
97/0/3	PA 6,6/POEMA/30B	97/0/3
95/0/5	PA 6,6/POEMA/30B	95/0/5
85/15/0	PA 6,6/POEMA/30B	85/15/0
82/15/3	PA 6,6/POEMA/30B	82/15/3
80/15/5	PA 6,6/POEMA/30B	80/15/5

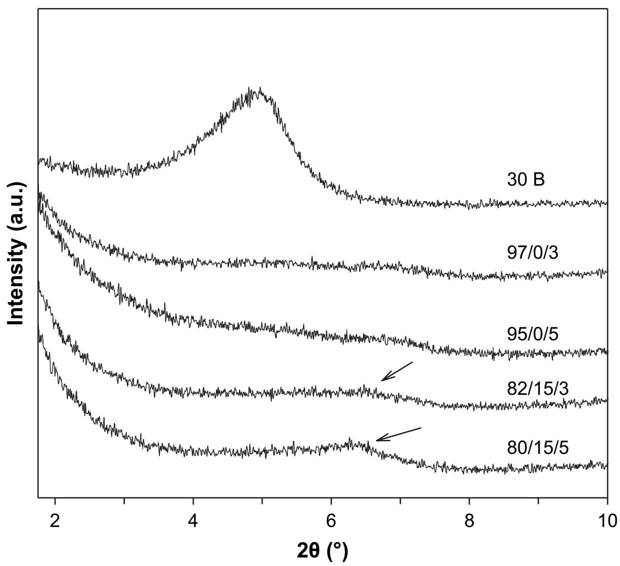

Fig. 1. XRD patterns of 30B and the prepared composites.

D5005 X-ray unit operating at 40 kV and 30 mA was used to carry out the XRD experiments at room temperature. The X-ray source was Cu Kα radiation with a wavelength of 1.54 Å. The diffractograms were scanned at a rate of 0.01°/s. The SEM/EDS experiments were performed on fractured surfaces of the samples with a combined JEOL JSM-5410 and JEOL 6587 system. The phase morphology of POEMA within the composites/blend was likewise evaluated by SEM. The TEM observations were performed on ultrathin sections of cryo-microtomed thin composite films with a JEOL JEM-2000EX II system using an acceleration voltage of 100 kV.

An Olympus BX-50 polarized light microscope (PLM) in conjunction with a Linkam THMS 600 hot stage was employed for the PA 6,6 crystalline morphology investigation of the samples. The thin-film specimens were prepared by first melting the samples and then compressing them between glass slides. The crystallization and melting behaviors of the samples were measured using a TA DSC Q10 analyzer equipped with an inter-cooler. To disclose the disintegration of PA 6,6 crystals during the melting process, in situ XRD experiments at a heating rate of 0.7 °C/min were carried out for neat PA 6,6 and selective composites. For the experiments, synchrotron X-ray measurements with a wavelength of 0.775 Å were performed at beamline BL01C of the National Synchrotron Radiation Research Center, Taiwan. The thermal stability of the samples was characterized using a thermogravimetric analyzer (TGA) on a TA Q50 system under an air environment. The heating process was conducted from room temperature to 700 °C at a rate of 10 °C/min.

The dynamic mechanical properties of compression-molded specimens were measured using a Perkin–Elmer DMA 7e system. The measurements were carried out in the three-point bending mode under a rate of 5 °C/min at a frequency of 1 Hz in an air atmosphere. Tensile properties of dog-bone-shaped specimens (according to the ASTM D638) were determined at a crosshead speed of 10 mm/min using a MTS Sintech 5/G system. Flexural modulus of the specimens was determined by the same MTS Sintech 5/G system at a crosshead speed of 2 mm/min. Notched Izod impact tests were performed using a CEAST impact tester in accordance with ASTM D256. The tensile/flexural properties and impact strength reported were averaged values from at least five specimens of the same sample.

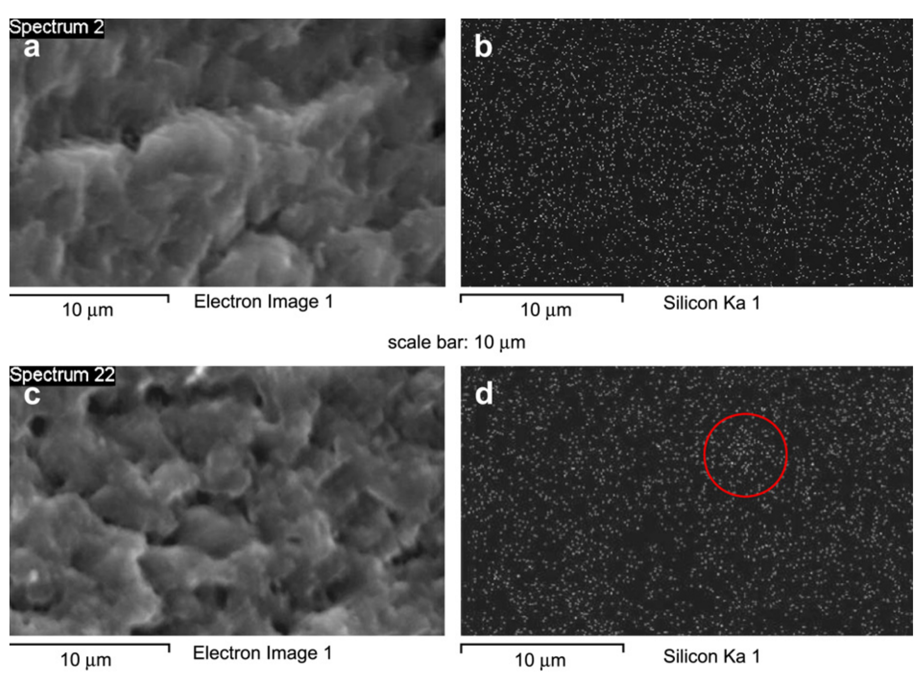

Fig. 2. (a) SEM micrograph of 95/0/5 composite; (b) EDS Si mapping of 95/0/5 composite; (c) SEM micrograph of 80/15/5 composite; (d) EDS Si mapping of 80/15/5 composite.

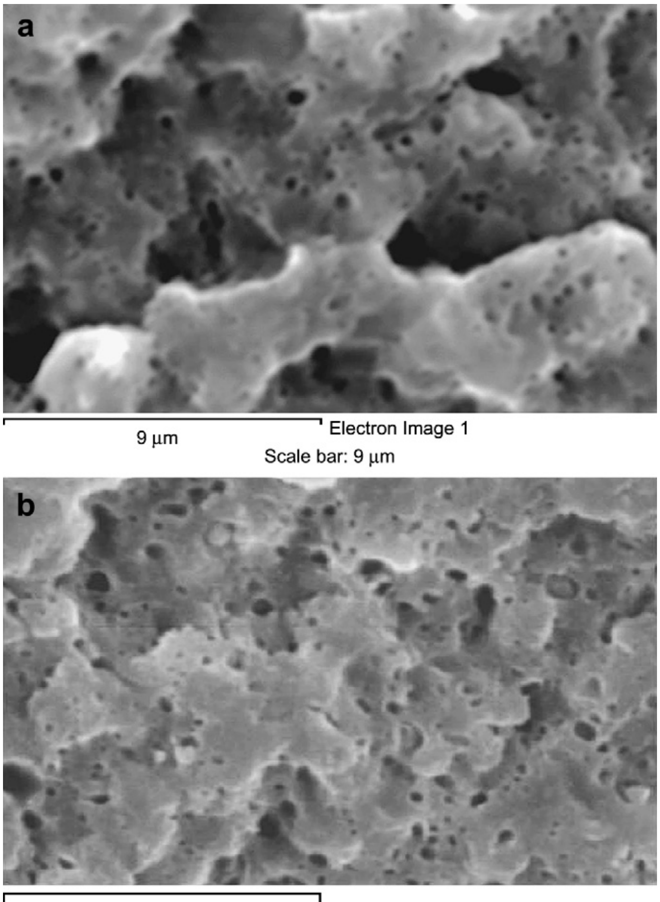

Fig. 3. (a) SEM micrograph of *p*-xylene-treated 85/15/0 blend; (b) SEM micrograph of *p*-xylene-treated 80/15/5 composite.

3. Results and discussion

3.1. Dispersibility of 30B in the composites

It is recognized that three types of clay-included composites can be classified: (1) conventional microcomposites, (2) partially exfoliated nanocomposites, including intercalated clays, and (3) fully exfoliated nanocomposites. The XRD technique is widely employed to examine the clay dispersibility. Fig. 1 shows the XRD patterns of neat 30B and the composites (in the 2θ range $<10°$). It is seen that the characteristic (001) diffraction peak of neat 30B is located evidently around $2\theta = 4.9°$ (*d*-spacing: 1.80 nm), whereas no discernible peak is observed for the 97/0/3 and 95/0/5 composites. This result suggests that the original layered-structure of 30B hardly exists in these two composites. The exfoliation and/or intercalation of 30B should have taken place during the mixing processes. However, shallow diffraction peaks of 30B located around $2\theta = 6.4°$ (*d*-spacing: 1.36 nm) are noticeable for the POEMA-included composites (cf. 82/15/3 and 80/15/5). These results indicate that the inclusion of POEMA had somehow depreciated the dispersibility of 30B in the PA 6,6 matrix, thereby suggesting that POEMA played little role in intercalating or exfoliating the 30B. The shift of 30B's diffraction to a higher angle means a reduction in 30B's interlayer spacing, which is believed to be caused by the partial decomposition of 30B's organic modifier during the mixing process [7].

To verify the dispersion status of 30B in the composites, SEM/EDS experiments were also carried out. Fig. 2(a–d) illustrates the representative SEM micrographs and their corresponding EDS Si mapping results of 95/0/5 and 80/15/5

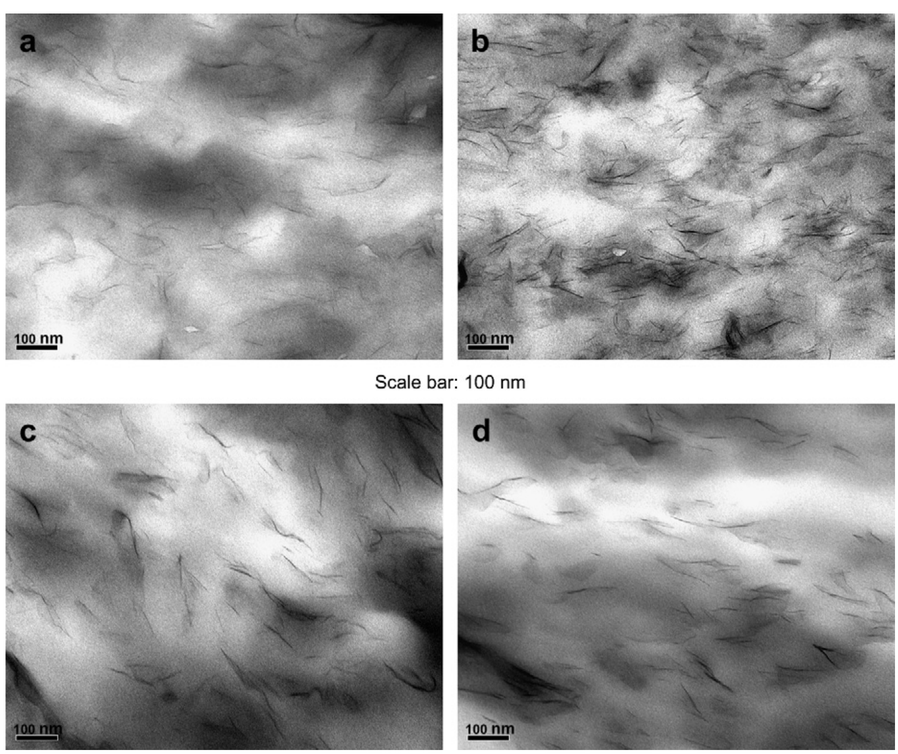

Fig. 4. TEM micrographs of the composites: (a) 97/0/3; (b) 95/0/5; (c) 82/15/3; (d) 80/15/5.

composites. The SEM micrographs show that no evident 30B aggregates are visible within the two samples. It is also noted that the POEMA phase is hardly detectable within the PA 6,6 matrix if no special treatment was conducted on the 80/15/5 composite. This is shown in Fig. 2(c). Regarding the light spots observed in EDS mapping results, they represent the locations of the Si element (from 30B). The uniformly distributed spots within the 95/0/5 composite suggest a homogeneous dispersion of 30B [28]. Nevertheless, a limited number of aggregated light spots (encircled area in Fig. 2(d)) seem to exist within the 80/15/5 composite, indicating an inferior dispersion of 30B within the POEMA-included composite. Based on the SEM/EDS results, it can be concluded that 30B was distributed finely in all the composites prepared. However, it was dispersed to a lesser extent in the POEMA-included composites. Furthermore, in order to ascertain the size and shape of distributed POEMA domains within the PA 6,6 matrix, with or without the presence of 30B, *p*-xylene was employed to etch out the POEMA phase in the composites/blend for SEM observations. Fig. 3(a and b) depicts the typical SEM micrographs of *p*-xylene-treated samples. The randomly distributed holes are clearly observed. The POEMA phase is thus confirmed to exhibit a sphere-like shape, with an average size smaller than 0.5 μm. The presence of a small amount of 30B seems to have little effect on the POEMA morphology in the PA 6,6 matrix.

The TEM experiments can provide a more detailed dispersion status for 30B in the composites. Fig. 4 displays TEM micrographs of 30B-included composites. The dark lines represent 30B while the white/gray base represents the polymer phase(s). In Fig. 4(a) and (b) (cf. 97/0/3 and 95/0/5 composites, respectively), the 30B is observed to be partially exfoliated into a thinner multi-layered structure or even a single layer. This indicates that a nano-scaled dispersion was achieved. Accordingly, no discernable (001) diffraction was observed in the corresponding XRD patterns. Fig. 4(c) and (d) illustrates the dispersion status of 30B in POEMA-included composites. Note that the presence of POEMA slightly altered the 30B dispersibility in the composites, that is, a more multi-layered structure of 30B exists, though these 30B aggregates

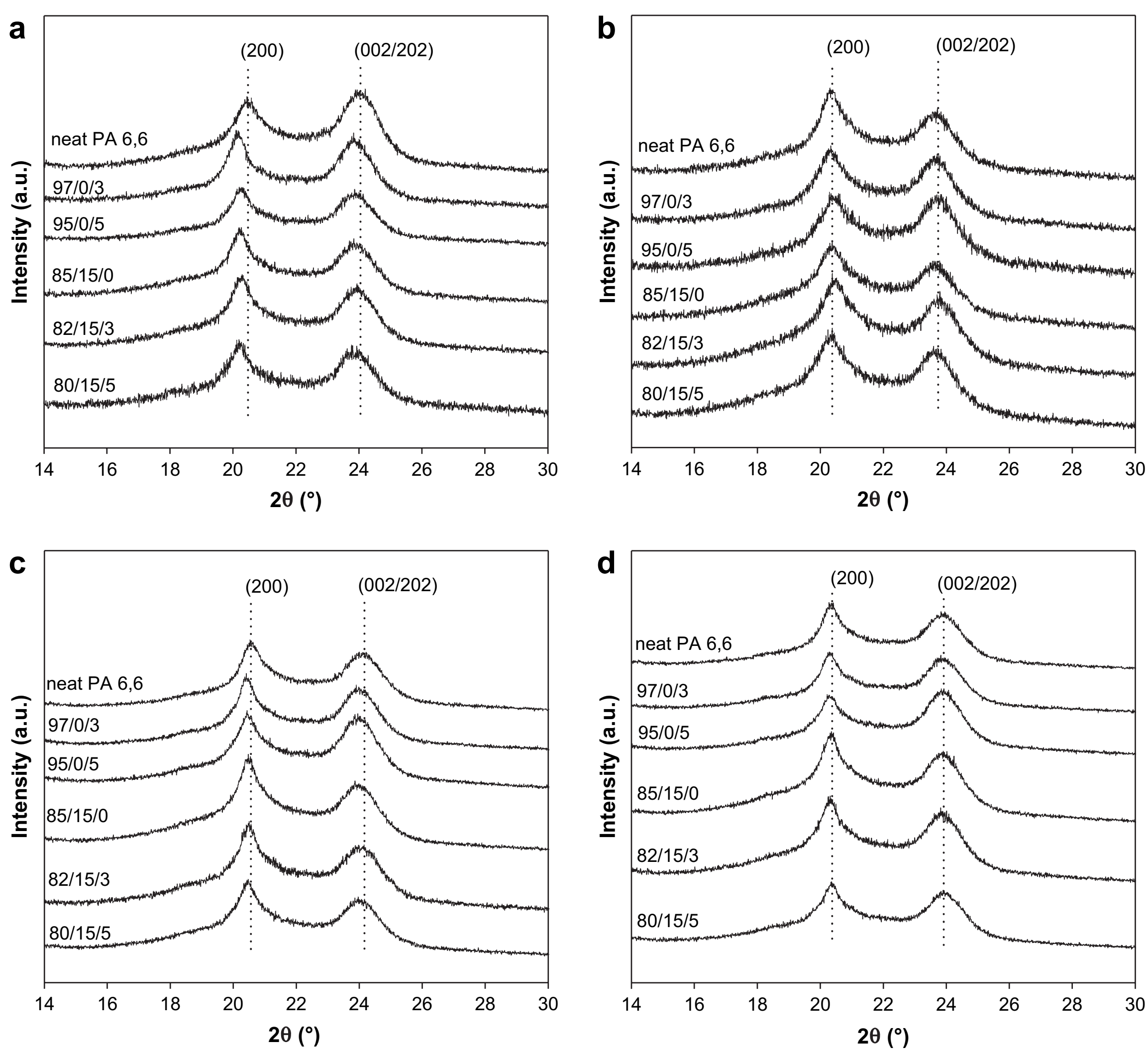

Fig. 5. XRD patterns of the samples: (a) cooled from the melt at 10 °C/min; (b) cooled from the melt by air-quenching; (c) isothermally crystallized at 245 °C; (d) isothermally crystallized at 239 °C.

are still distributed randomly in the matrix. In addition, their layered-structure thicknesses are mainly less than 100 nm. As a consequence, a shallow (001) diffraction peak was observed in the corresponding XRD pattern for each POEMA-included composite. Through the 30B dispersibility observations using different techniques, it can be concluded that various PA 6,6-based nanocomposites were developed.

3.2. Crystal structure

PA 6,6 has been reported to exhibit two main crystalline forms, termed α and γ. The triclinic α-form is composed of planar sheets of hydrogen bonding chains with sheets stacked upon one another along the chain direction. The triclinic (pseudohexagonal) γ-form consists of pleated sheets of methylene units with hydrogen bonding between sheets rather than within the sheets. Of the two forms, the α-form is recognized as thermodynamically stable. Furthermore, it can transform to the γ-form at elevated temperatures. The characteristic XRD peaks of the α-form crystal are located around $2\theta = 20°$ and $24°$ ($\lambda = 1.54$ Å), and indexed as (200) and (002/202) diffractions, respectively [16]. For the γ-form, one peak mainly shows up around $2\theta = 22°$. Fig. 5 shows the room temperature XRD patterns of different thermally treated samples. It is evident that PA 6,6 predominantly exhibits the α crystalline structure regardless of the thermal treatments and the presence of 30B and/or POEMA. However, if we compare the diffraction patterns of neat PA 6,6 with other samples in more detail, we can find that the presence of 30B and/or POEMA may slightly affect the crystal structure of PA 6,6 depending on the thermal treatment. That is, when the samples were crystallized slowly (Fig. 5(a) and (c)), the two characteristic diffraction peaks of the α-form crystal shift to lower angles with the presence of 30B and/or POEMA. The shifts mean the distance expansions of (200) planes and (002/202) planes, which might be due to the affinity (interaction) between PA 6,6 chains and 30B/POEMA upon crystallization. Nevertheless, the d-spacings of (200) and (002/202) planes are almost maintained (no diffraction peaks shift) if the samples were crystallized under faster rates (Fig. 5(b) and (d)). This observation suggests that lesser interactions between PA 6,6 chains and 30B/POEMA were involved in the formation of PA 6,6 crystals once the crystals were grown rapidly.

3.3. Crystallization and melting behaviors

Fig. 6(a) shows the DSC cooling thermograms of the samples at a rate of 10 °C/min. It is found that the crystallization peak temperature (T_p, temperature at the exotherm minimum) of neat PA 6,6 is around 233 °C, whereas the T_p shifts to higher temperatures with the addition of 30B exclusively. The 30B thus played the role of a nucleation agent for PA 6,6. Furthermore, it is noted that the T_p of the 97/0/3 sample is slightly higher than that of the 95/0/5 sample. The reason for this might be due to the fact that a higher exfoliated/intercalated 30B content not only induced the heterogeneous nucleation for PA 6,6 upon crystallization, but also caused a confined/constrained environment for retarded crystallization of PA 6,6 chains. Regarding the effect of adding POEMA (cf. 85/15/0 blend), it is found that the T_p of PA 6,6 is hardly influenced. For the samples containing a co-existing 30B and POEMA, the T_p of PA 6,6 shifts to lower temperatures, especially for the 80/15/5 sample. Accordingly, the simultaneous incorporations of 15% of POEMA and 5% of 30B into PA 6,6 must have induced a higher degree of interaction between themselves and PA 6,6 molecules, which causes impeded chain mobility in PA 6,6 upon crystallization. Consequently, the accelerating nucleation effect of 30B on PA 6,6 crystallization is obscured and not seen. In addition, the crystallization enthalpy (ΔH_c) of PA 6,6 is found to decrease with the presence of POEMA, while the value changes little with the addition of 30B exclusively. For the samples cooled at the rate of 40 °C/min (Fig. 6(b)), similar behaviors are observed, except

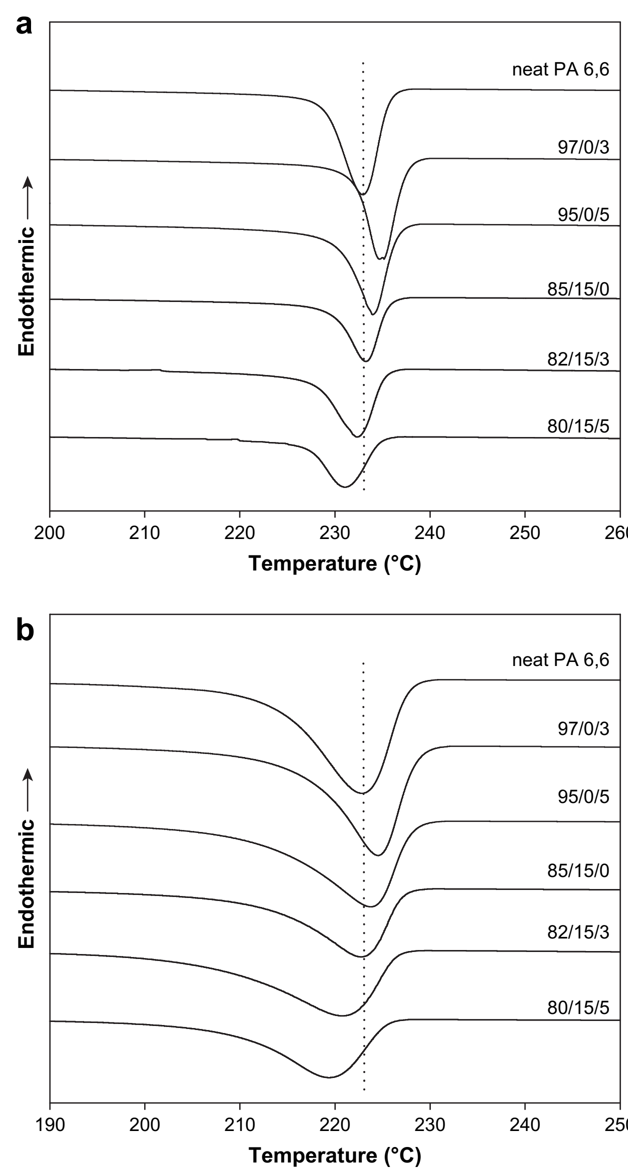

Fig. 6. DSC cooling thermograms of the samples: (a) at 10 °C/min cooling rate; (b) at 40 °C/min cooling rate.

Table 2
Some representative thermal and mechanical data of the samples

Properties	Samples					
	Neat PA 6,6	97/0/3	95/0/5	85/15/0	82/15/3	80/15/5
T_p[a] (°C)	232.9	235.8	234.3	233.1	232.2	231.0
ΔH_c[a] (J/g)	62.2	64.5	62.1	43.4	44.9	43.1
T_p[b] (°C)	222.8	224.9	223.9	222.4	220.4	219.2
ΔH_c[b] (J/g)	63.8	64.3	60.1	45.3	43.7	45.3
$T_{d(5\%)}$[c] (°C)	371.1	377.8	380.3	391.2	392.5	390.3
$T_{d(25\%)}$[c] (°C)	386.0	412.6	421.6	422.1	428.1	426.7
T_{max} (°C)	399.5	440.5	441.1	441.3	447.0	443.5
YM (GPa)	1.46	1.70	1.75	1.07	1.19	1.22
TS (MPa)	43.6	48.2	50.1	44.7	46.5	47.4
EB (%)	57.7	3.5	3.7	113.5	62.3	38.7
FM (GPa)	2.32	2.45	2.65	1.45	1.65	1.75
IS (J/m)	39.9	20.9	20.1	133.1	75.4	56.1

[a] 10 °C/min-cooled.
[b] 40 °C/min-cooled.
[c] $T_{d(\alpha\%)}$: decomposition temperature at α% weight loss.

for the T_p's shift to lower temperatures. The T_ps and ΔH_cs of PA 6,6 in the samples are included in Table 2.

Fig. 7 illustrates the DSC heating thermograms of 10 °C/min melt-crystallized samples under a heating rate of 20 °C/min. Complex melting behaviors, a low melting-temperature ($T_{m,1}$) peak (denoted as peak I), and a high melting-temperature ($T_{m,2}$) peak (denoted as peak II) of PA 6,6 in the pure state and in the composites/blend are observed. It is also noticed that the $T_{m,2}$s of 30B-included composites are lower than those of other samples, while the $T_{m,1}$s of all the samples are close to one another. Moreover, the intensity ratio of peak I to peak II is slightly higher for the 30B-included composites. According to the above XRD results, the complex melting behavior is unlikely to stem from different PA 6,6 polymorphs. In order to disclose the origin of the complex melting behavior, different heating rates were employed in the DSC experiments. Fig. 8(a and b) illustrates the DSC heating thermograms of 40 °C/min melt-crystallized neat PA 6,6 and 97/0/3 composites under different heating rates, respectively. It is found that the gap between the two melting peaks becomes narrow for both of the samples as the heating rate increases, that is, partially overlapped peaks are exhibited in the thermograms, especially for the samples scanned at faster rates. After analyzing the overlapped peaks carefully, it is found that a faster heating rate causes an increase in the peak intensity ratio between peak I and peak II. The thermal lag-induced melting peaks that slightly shift to higher temperatures along with the heating rate is also observed. The above results suggest that the occurrence of peak II is mainly due to the crystal annealing effect during the heating scans. That is to say, the recrystallization and/or reorganization of PA 6,6 molecules in the crystals would occur upon the heating processes if the originally formed crystals were not stable enough. Accordingly, the recrystallization and/or reorganization processes become less evident as the heating rate rises, which results in a relatively higher intensity ratio between peak I and peak II. As the

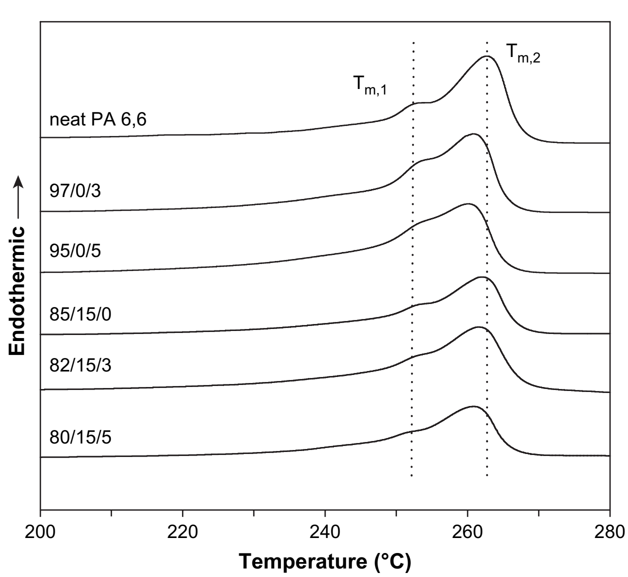

Fig. 7. DSC heating thermograms of 10 °C/min-cooled samples.

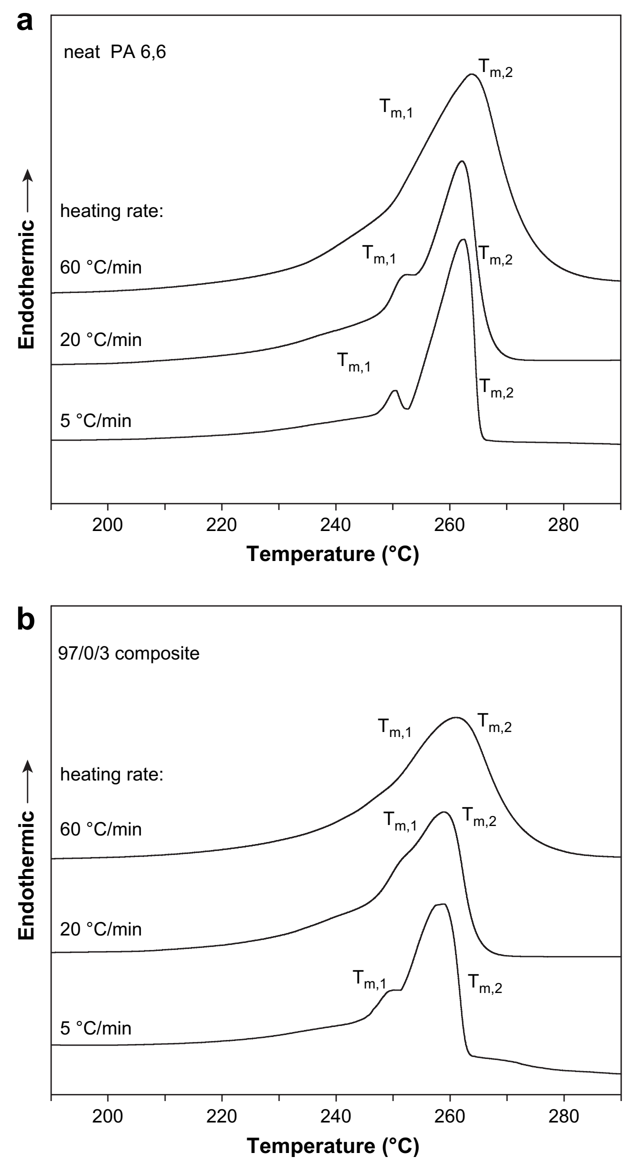

Fig. 8. DSC heating thermograms of 40 °C/min-cooled samples at different heating rates: (a) neat PA 6,6; (b) 97/0/3 composite.

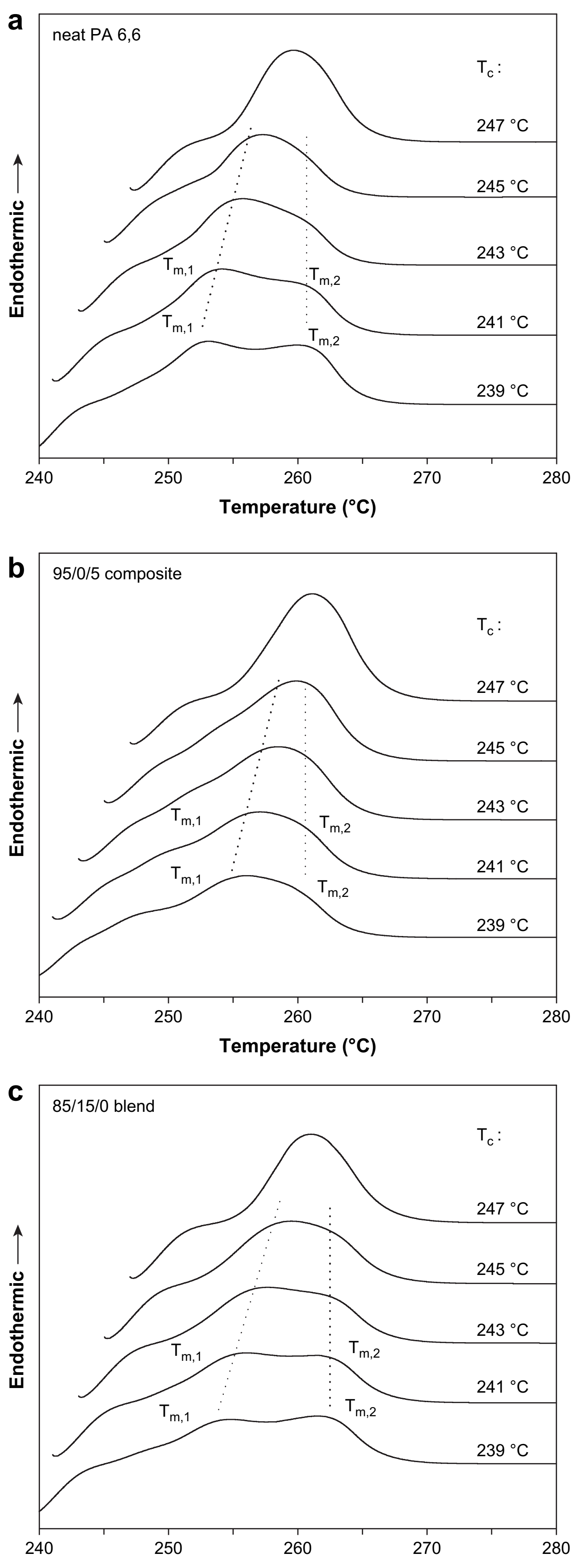

Fig. 9. DSC heating thermograms of isothermally crystallized samples: (a) neat PA 6,6; (b) 95/0/5 composite; (c) 85/15/0 blend.

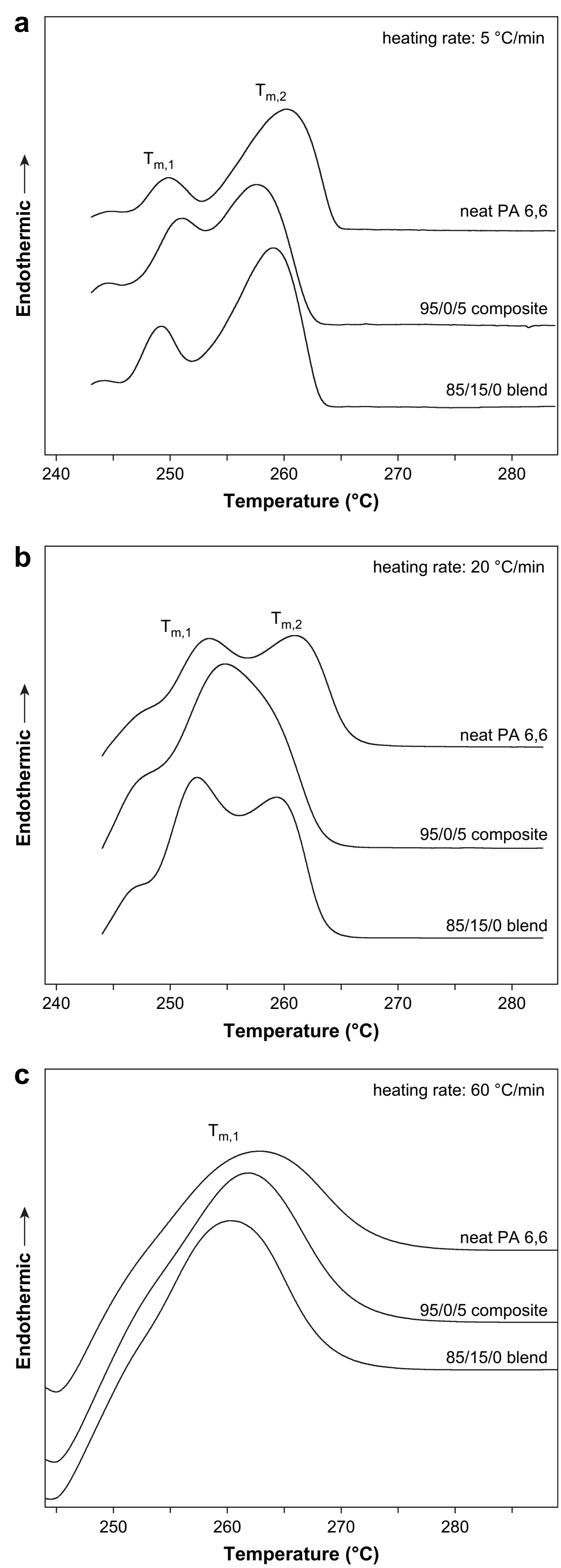

Fig. 10. DSC heating thermograms of $T_c = 239$ °C crystallized three samples at different heating rates: (a) 5 °C/min; (b) 20 °C/min; (c) 60 °C/min.

reason causing the complex melting behavior is recognized, the thermograms in Fig. 7 imply that the crystals' annealing effect declines with the incorporation of 30B in the samples. A similar phenomenon can be also observed in Fig. 8. The exfoliated/intercalated 30B should somehow inhibit the recrystallization and/or the reorganization of the originally formed PA 6,6 crystals. The recrystallized and/or reorganized crystals thus exhibit lesser stability, causing the lower $T_{m,2}$s in turn.

To further reveal the influences of adding 30B and POEMA on the melting behavior of the PA 6,6 matrix, Fig. 9(a–c) depicts the representative DSC melting thermograms of three samples, namely, neat PA 6,6, 95/0/5 composite, and 85/15/0 blend, which were isothermally crystallized at various temperatures (T_cs). Some features are worth noting in these melting thermograms. First, two partially overlapped melting peaks are observed for the three samples crystallized at lower T_cs, whereas only one broad melting peak shows up for higher T_c-crystallized samples. Second, if two melting peaks are evident in the thermograms, then the low melting-temperature peak (peak I) shifts to a higher temperature with T_c. However, the high melting-temperature peak (peak II) changes little. Third, the intensity ratio between peak I and peak II increases with T_c. In fact, the three noted phenomena suggest the above conclusion regarding the origin of the complex melting behavior. Fig. 10 shows the DSC melting thermograms of the three samples, isothermally crystallized at 239 °C, under three different heating rates. The occurrence of recrystallization and/or reorganization of PA 6,6 crystals is further confirmed for neat PA 6,6 and the composite/blend, especially at a slower heating rate of 5 °C/min. While comparing the thermograms in Figs. 9 and 10, in more detail, it is further noticed that if the three samples were crystallized at the same T_c, the melting behaviors of neat PA 6,6 and 85/15/0 blend resemble each other, while they are, at the same time, different from that of the 95/0/5 composite. That is, the intensity ratio of peak I to peak II is higher for the 30B-included composite, which is consistent with previous melting behavior results (non-isothermally crystallized samples). From the DSC analyses, it can be concluded that the addition of 30B would bring about a noticeable effect on the melting behavior of PA 6,6. Moreover, the addition of POEMA had little influence on the melting behavior of PA 6,6.

Fig. 11 illustrates the selective temperature-dependent (in situ) XRD patterns of neat PA 6,6 and 95/0/5 composite (40 °C/min-cooled from the melt) upon heating, and their corresponding diffraction peak intensity versus temperature as well. As anticipated, the α-form PA 6,6 crystals associated two diffractions transform to the γ-form crystals related one diffraction during the heating processes for both samples. The composite is found to exhibit a lower α- to γ-form transition temperature (Brill transition) than that of neat PA 6,6, which is consistent with that reported by Liu et al. [16]. The figure of γ-form diffraction peak intensity versus temperature (cf. Fig. 11(b)) shows that the intensity of the two samples declines gradually with temperature during the melting processes. Nevertheless, the intensity of neat PA 6,6 displays a discontinuity between 250 and 255 °C, which may be ascribed to the occurrence of recrystallization and/or reorganization of PA 6,6 molecules [29]. The 95/0/5 composite does not exhibit a discontinuity likewise because its recrystallization and/or reorganization processes are somehow hampered by the exfoliated/intercalated 30B as suggested by the DSC results.

3.4. Thermal stability

The TGA-scanned results of the samples are shown in Fig. 12(a). Some observations can be made. First, all of the samples display a similar single-step degradation process. Second, the neat PA 6,6 exhibits the least thermal stability among the samples. For instance, the PA 6,6 starts to degrade around 370 °C, whereas the degradation temperatures of the other samples are around or above 380 °C. Third, the thermal stability of the composites and the blend resembles one another and is slightly higher than that of neat POEMA. The TGA results evidently indicate that the thermal stability of PA 6,6 was enhanced after adding 30B and/or POEMA. The phenomenon of similar degradation behaviors exhibited by the composites and the blend could be attributed to their comparable 30B/POEMA dispersion status within the PA 6,6 matrix. The thermal stability enhancement is a consequence of the homogeneous dispersion of layered-30B and POEMA, which results in oxygen and heat permeability reductions in the PA 6,6 matrix during the heating scans. The corresponding derivative TGA (DTGA) curves of the samples are shown in Fig. 12(b). The PA 6,6 shows the lowest peak temperature (T_{max}, temperature at the maximum weight loss rate) among the samples. With the incorporations of 30B and/or POEMA, the peak height decreases and the peak width broadens as well. These results further suggest the thermal stability enhancement of PA 6,6 in the composites/blend. Some representative TGA data are listed in Table 2.

3.5. Crystalline morphology

The PA 6,6 crystalline morphology of 10 °C/min melt-crystallized samples is observed through PLM as depicted in Fig. 13(a–f). Typical spherulites with Maltese cross are grown in neat PA 6,6. After adding 30B, the PA 6,6 spherulites become diffused and smaller, which implies the accelerated PA 6,6 nucleation by 30B. This observation is basically in agreement with the DSC crystallization results. It has been further observed that many dark spots are exhibited within the PA 6,6 spherulites after the addition of POEMA exclusively (cf. Fig. 13(d)). The spherulites' size becomes slightly smaller than that of neat PA 6,6. The dark spots indeed represent the POEMA. This means that POEMA component could be included within the PA 6,6 spherulites. For the PA 6,6/POEMA/30B composites (cf. Fig. 13(e and f)), broken/diffused spherulites with POEMA inclusion are developed. The boundary among the crystallites (e.g., spherulites) becomes indistinct. A similar evolution of PA 6,6 crystalline morphology with the additions of 30B and/or POEMA is observed for 40 °C/min melt-crystallized samples, too (not shown here for

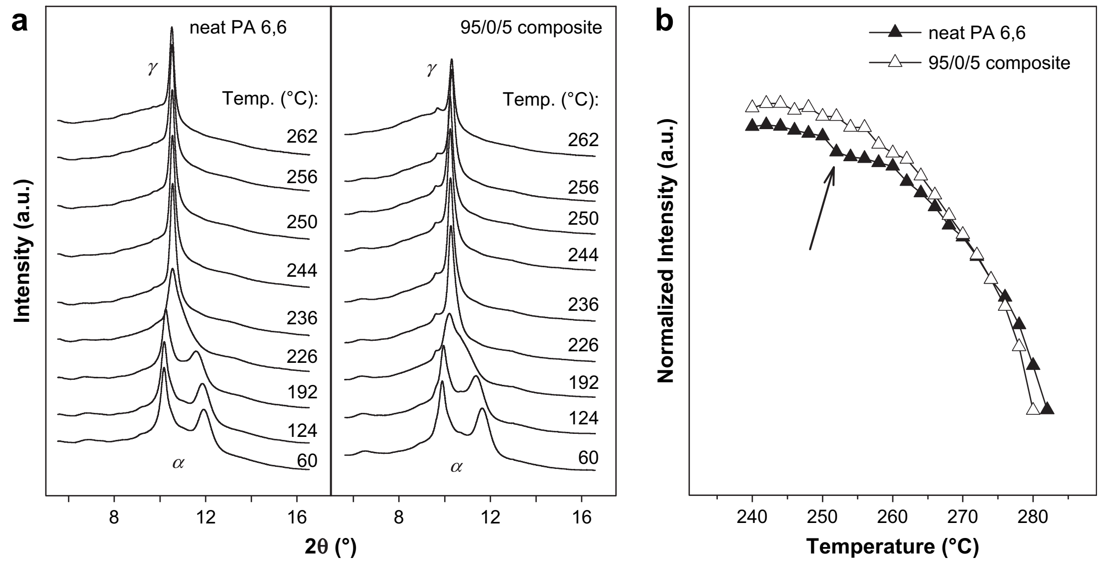

Fig. 11. (a) Temperature-dependent (in situ) XRD patterns of neat PA 6,6 and 95/0/5 composite; (b) the γ-form diffraction peak intensity versus temperature for the two samples.

brevity). The observed difference is that the average crystallites' size declines due to a faster cooling rate.

3.6. Mechanical properties

The storage modulus (E') of the samples was examined by DMA as depicted in Fig. 14. The samples are noted to exhibit similar decreasing E' trends with increasing temperature. This behavior is due to the increase in segmental PA 6,6 chain motion with temperature. In the 50–100 °C range, the evident E' drop demonstrates the glass transition of PA 6,6. It is worth noting that the PA 6,6/30B composites (97/0/3 and 95/0/5) show higher E' values than those of the other samples and that the value increases with a higher 30B content. This evident E' reinforcement stems from the nano-scaled dispersion of 30B within the PA 6,6 matrix. In contrast, for the PA 6,6/POEMA blend, its E' values are lower than those of other samples. This result is caused by the elastomeric nature of POEMA. As for the composites, including both 30B and POEMA, their E' values are similar to one another. In addition, the E' values are lower than those of neat PA 6,6, but higher than those of the PA 6,6/POEMA blend. This behavior suggests that POEMA played a more important role than 30B in controlling the E' of the samples. The loss tangent (tan δ) of the samples at various temperatures is also evaluated. The dynamic relaxation peak temperatures (i.e., glass transition temperatures, T_gs) of the 30B-included composites are found to be slightly higher than those for neat PA 6,6 and the PA 6,6/POEMA blend, up to 3–4 °C.

In addition to the dynamic mechanical properties, the tensile and flexural properties of the samples were measured. The measured Young's modulus (YM), tensile strength (TS),

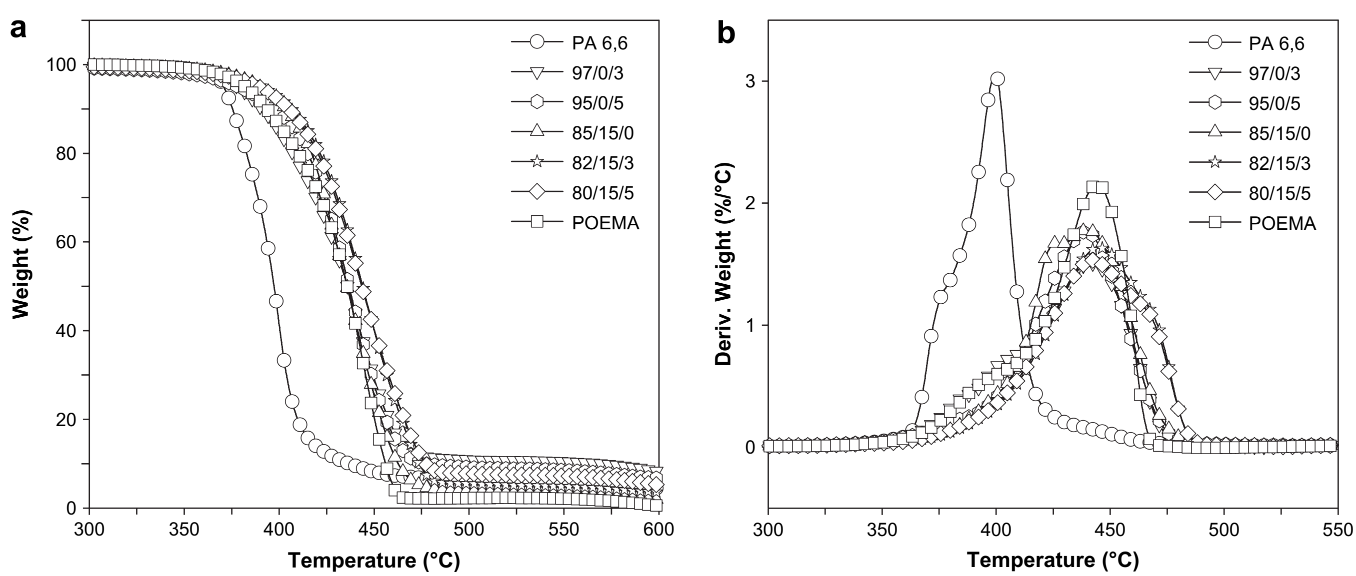

Fig. 12. (a) TGA decomposition curves of the samples; (b) DTGA curves of the samples.

elongation at break (EB), and flexural modulus (FM) are listed in Table 2. It is evident that adding 30B increases the Young's modulus, tensile strength, and flexural modulus of PA 6,6 (cf. PA 6,6/30B composites). However, the elongation at break is inversely affected. With the incorporation of POEMA into the PA 6,6 matrix (cf. PA 6,6/POEMA blend), the Young's modulus, tensile strength, and flexural modulus decline, stemming from the elastomeric nature of POEMA. For the two PA 6,6/POEMA/30B composites, their tensile/flexural properties fall between those of the neat PA 6,6 and PA 6,6/POEMA blend.

Izod impact tests were carried out to determine the effects of adding 30B and/or POEMA on the samples' toughness. The results are included in Table 2, which reveal that after adding 30B the impact strength (IS) of PA 6,6 decreases *ca*. 50%, reaching a value of 20.1 J/m. Conversely, the incorporation of POEMA results in a 2.33 times increase in PA 6,6 impact strength (up to 133.1 J/m), indicating an apparently

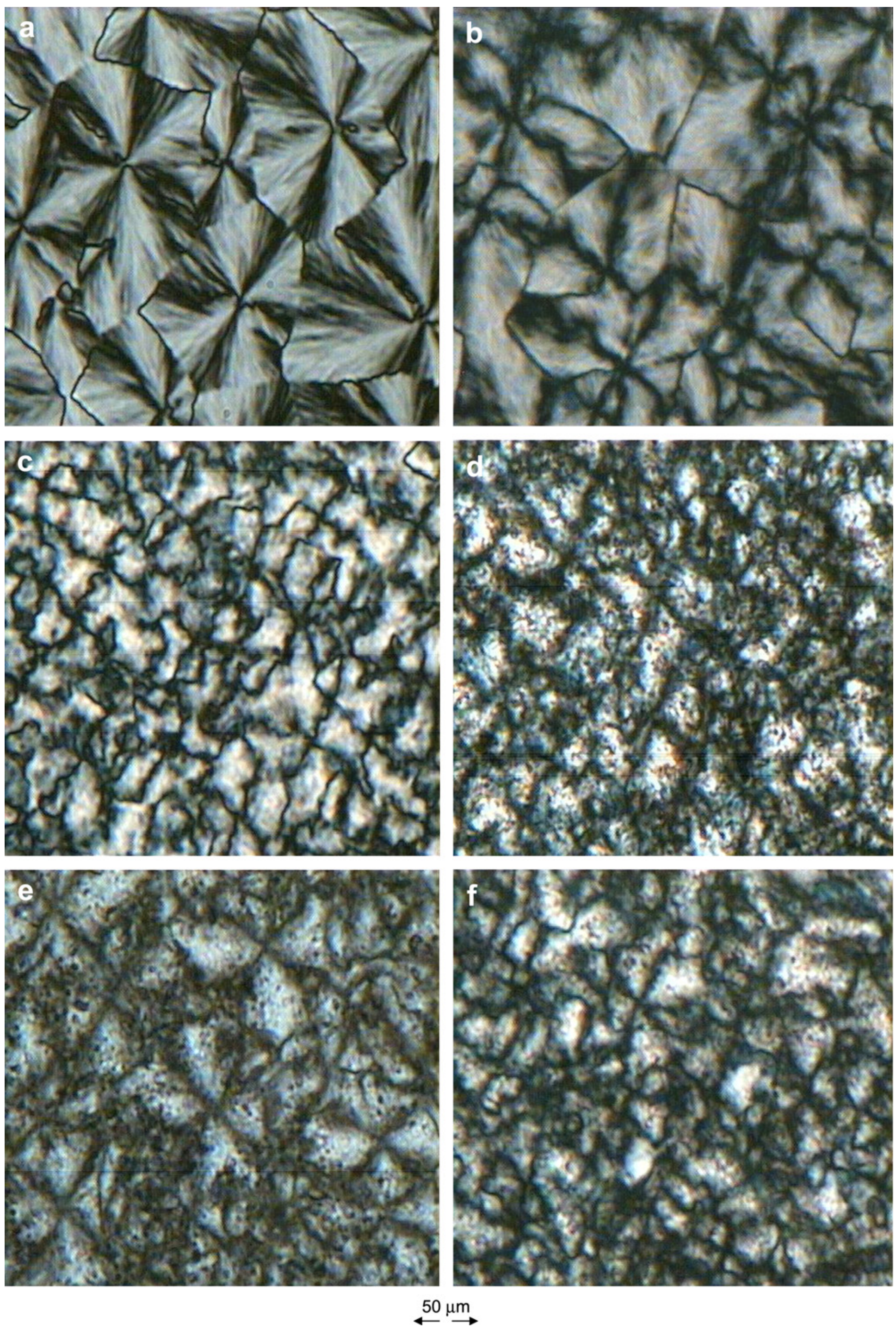

Fig. 13. PLM micrographs of the samples: (a) neat PA 6,6; (b) 97/0/3 composite; (c) 95/0/5 composite; (d) 85/15/0 blend; (e) 82/15/3 composite; (f) 80/15/5 composite.

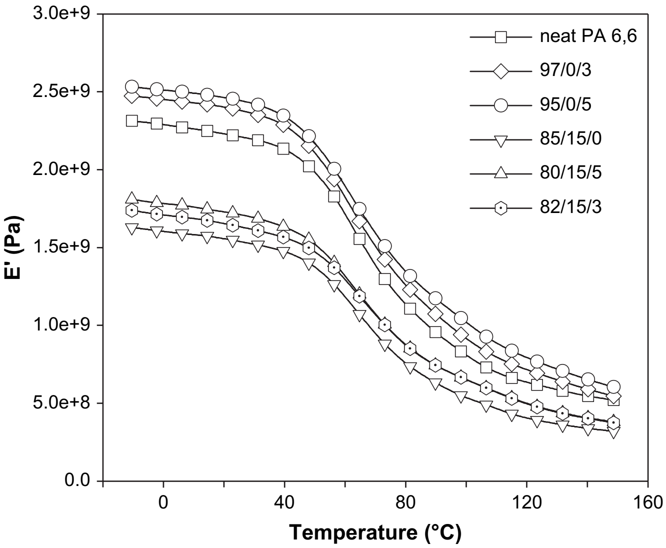

Fig. 14. DMA results of E' versus temperature for the samples.

toughening effect. The reason for this remarkable enhancement is believed to be associated with the interactions between the MA portion of POEMA and the amino group of PA 6,6. For the composites with both 30B and POEMA inclusions, balanced impact strengths are observed. Their impact strengths are higher than that of neat PA 6,6, but lower than that of the PA 6,6/POEMA blend.

4. Conclusions

The dispersibility of a commercial O-MMT (30B) within a PA 6,6 matrix in the absence or presence of a POEMA elastomer was evaluated in this study. The thermal/mechanical properties and crystalline morphology of the melt-mixed samples were determined as well. XRD, SEM/EDS, and TEM results indicated that the layered-30B was exfoliated (or at least intercalated) in the prepared composites. The PA 6,6-based nanocomposites were thus achieved. Nevertheless, the incorporation of POEMA in the nanocomposites slightly depreciated the dispersibility of 30B. The incorporations of 30B and/or POEMA did not change the crystalline polymorph of PA 6,6 at room temperature. The α-form crystals predominantly existed in the prepared samples, with the possibility that the *d*-spacings of (200) and (002/202) might expand after adding 30B. The α-form PA 6,6 crystals transformed to γ-form crystals during the heating scans as revealed by in situ XRD experiments; the presence of 30B lowered the Brill transition temperature. The crystallization kinetics of PA 6,6 was altered as 30B was added. It was because 30B might play the role of a nucleation agent and also afforded a confined/constrained environment for the PA 6,6 crystallization. The complex DSC melting behaviors observed for the samples were attributed to the occurrence of the "recrystallization and/or reorganization" process of PA 6,6 crystals. The presence of 30B would decline the extent of the "recrystallization and/or reorganization" process. The TGA data confirmed the thermal stability enhancement of PA 6,6 after adding 30B and/or POEMA. The storage/Young's/flexural moduli and tensile strength of PA 6,6 increased with the inclusion of 30B. However, the addition of POEMA produced a decrease in these properties. Conversely, 30B and POEMA additions produced a reverse effect on the PA 6,6 toughness. The PA 6,6/POEMA/30B nanocomposites basically presented balanced mechanical properties between those of the neat PA 6,6 and PA 6,6/POEMA blend.

Acknowledgements

The authors would like to thank the National Science Council of the Republic of China (Taiwan) for financially supporting this research under contract number NSC-93-2622-E-182-002-CC3.

References

[1] Usuki A, Kojima Y, Kawasumi M, Okada A, Fukushima Y, Kurauchi T, et al. J Mater Res 1993;8:1179.
[2] Kojima Y, Usuki A, Kawasumi M, Okada A, Kurauchi T, Kamigaito O. J Polym Sci Polym Chem Ed 1993;31:983.
[3] Vaia RA, Jandt KD, Kramer EJ, Giannelis EP. Macromolecules 1995; 28:8080.
[4] Lincoln DM, Vaia RA, Wang ZG, Hsiao BS. Polymer 2001;42:1621.
[5] Ratna D, Divekar S, Samui AB, Chakraborty BC, Banthia AK. Polymer 2006;47:4068.
[6] Wang K, Wang C, Li J, Su J, Zhang Q, Du R, et al. Polymer 2007;48:2144.
[7] Chiu FC, Lai SM, Chen JW, Chu PH. J Polym Sci Polym Phys Ed 2004;42:4139.
[8] Masenelli-Varlot K, Vigier G, Vermogen A, Gauthier C, Cavaille JY. J Polym Sci Polym Phys Ed 2007;45:1243.
[9] Wang Y, Zhang Q, Fu Q. Macromol Rapid Commun 2003;24:231.
[10] Shah RK, Paul DR. Polymer 2006;47:4075.
[11] Chiu FC, Lai SM, Chen YL, Lee TH. Polymer 2005;46:11600.
[12] Chiu FC, Chu PH. J Polym Res 2006;13:73.
[13] Lincoln DM, Vaia RA, Wang ZG, Hsiao BS, Krishnamoorti R. Polymer 2001;42:9975.
[14] Homminga D, Goderis B, Dolbnya I, Groeninckx G. Polymer 2006;47: 1620.
[15] Malucelli G, Ronchetti S, Lak N, Priola A, Dintcheva NT, La Mantia FP. Eur Polym J 2007;43:328.
[16] Liu X, Wu Q, Berglund LA. Polymer 2002;43:4967.
[17] Yu ZZ, Yan C, Yang M, Mai YW. Polym Int 2004;53:1093.
[18] Zhang QX, Yu ZZ, Yang M, Ma J, Mai YW. J Polym Sci Polym Phys Ed 2003;41:2861.
[19] Kang X, He S, Zhu C, Lu LWL, Guo J. J Appl Polym Sci 2005;95:756.
[20] Nair SV, Goettler LA, Lysek BA. Polym Eng Sci 2002;42:1872.
[21] Oshinski AJ, Keskkula H, Paul DR. Polymer 1992;33:284.
[22] Muratoglu OK, Argon AS, Cohen RE, Weinberg M. Polymer 1995;36:4771.
[23] Ban LL, Doyle MJ, Disko MM, Smith GR. Polym Commun 1988;29: 163.
[24] Sun SL, Tan ZY, Xu XF, Zhou C, Ao YH, Zhang HX. J Polym Sci Polym Phys Ed 2005;43:2170.
[25] Huang JJ, Keskkula H, Paul DR. Polymer 2006;47:639.
[26] Wahit MU, Hassan A, Ishak ZAM, Rahmat AR, Othman N. Polym J 2006;38:767.
[27] Yu ZZ, Ke YC, Ou YC, Hu GH. J Appl Polym Sci 2000;76:1285.
[28] Sengupta R, Bandyopadhyay A, Sabharwal S, Chaki TK, Bhowmick AK. Polymer 2005;46:3343.
[29] Chuang WT, Hong PD, Chen CH, Sheu HS, Jeng US. J Appl Crystallogr 2007;40(S1):S637.